Agricultural and Forest Meteorology 308-309 (2021) 108600

Contents lists available at ScienceDirect

Agricultural and Forest Meteorology

journal homepage: www.elsevier.com/locate/agrformet

# Large methane emission from freshwater aquaculture ponds revealed by long-term eddy covariance observation

Jiayu Zhao [a,b], Mi Zhang [b,c,*], Wei Xiao [b,c], Lei Jia [b], Xiufang Zhang [b,e], Jiao Wang [b,f], Zhen Zhang [b,g], Yanhong Xie [b], Yini Pu [b], Shoudong Liu [b], Zhaozhong Feng [h], Xuhui Lee [d,*]

[a] School of Environmental Science and Engineering, Nanjing University of Information Science and Technology, Nanjing, Jiangsu Province, China
[b] Yale-NUIST Center on Atmospheric Environment, International Joint Laboratory on Climate and Environment Change (ILCEC), Nanjing University of Information Science and Technology, Nanjing, Jiangsu Province, China
[c] Key Laboratory of Meteorological Disaster, Ministry of Education and Collaborative Innovation Center on Forecast and Evaluation of Meteorological Disasters, Nanjing University of Information Science and Technology, Nanjing, Jiangsu Province, China
[d] School of the Environment, Yale University, New Haven, CT, United States
[e] Yunnan Meteorological Service Center, Kunming, Yunnan Province, China
[f] Taiyuan Meteorological Bureau, Taiyuan, Shanxi Province, China
[g] Nanjing Jiangning District Meteorological Bureau, Nanjing, Jiangsu Province, China
[h] Key Laboratory of Agrometeorology of Jiangsu Province, Institute of Ecology, School of Applied Meteorology, Nanjing University of Information Science and Technology, Nanjing, Jiangsu Province, China

ARTICLE INFO

*Keywords:*
Aquaculture pond
Eddy covariance method
Methane flux

ABSTRACT

Aquaculture ponds are important anthropogenic methane ($CH_4$) sources to the atmosphere. Currently large uncertainties still remain regarding the emission strength of this source type and its relationship with aquacultural farming practices. In this study, the methane flux was measured continuously for four years with eddy covariance (EC) in an aquaculture pond complex in the Yangtze River Delta, China. These ponds have never been dredged and were aerated during part of the aquacultural season. Additionally, floating chambers and inverted funnels were used to investigate spatial heterogeneity of the $CH_4$ flux and to quantify the contribution via ebullition to the flux. The results showed that the daily $CH_4$ flux ranged from 0.1 to 16.7 μg $m^{-2}$ $s^{-1}$, with an average value of 4.10 ± 3.08 μg $m^{-2}$ $s^{-1}$. Water temperature was the primary driver of the $CH_4$ flux across multiple time scales (half-hourly, daily, and monthly scale). Ebullition was the main transport way accounting for 70% ± 4% of the total $CH_4$ flux. The annual flux in this study was about three times the median flux reported by other researchers for similar freshwater aquaculture ponds. A statistical analysis of our data together with the published flux data reveals that ponds with dredging have much lower $CH_4$ emission flux than those without dredging and suggests that dredging may have a much larger influence on the emission flux than aeration.

## 1. Introduction

Aquaculture accounts for nearly half of the global fish production, providing an important source of protein for the world's population (FAO, 2020). Aquaculture ponds are hotspots of anthropogenic $CH_4$ emission because they receive substantial loads of allochthonous carbon through frequent addition of feed material (Liu et al., 2016; Yang et al., 2017, 2018, 2019; Yuan et al., 2019; Kosten et al., 2020; Yang et al., 2020; Peacock et al., 2021; Rosentreter et al., 2021; Yuan et al., 2021). These ponds are either fully enclosed with no outflow or semi-enclosed with minimal water discharge to neighboring lands, with a depth typically in the range of 1 to 2 m (Boyd et al., 2010; Adhikari et al., 2012; Yang et al., 2020). Like natural water bodies, $CH_4$ in these ponds is produced by methanogens in the sediment under anaerobic conditions. Some of the $CH_4$ is oxidized in the water column, and the rest escapes to the atmosphere by diffusion and ebullition (Bastviken et al., 2004). In natural waters, $CH_4$ production is fueled by in-situ primary production through photosynthesis or by organic matter input via river channels. In aquaculture systems, fish feed is the main source of organic matter for $CH_4$ production. The annual amount of fish feed ranges from 120 to 1600 g C $m^{-2}$ $y^{-1}$ (Liu et al., 2016; Ma et al., 2018; Wu et al., 2018; Yuan et al., 2019; Adhikari et al., 2020). In comparison, C input in lakes and

* Corresponding authors.
*E-mail addresses:* zhangm.80@nuist.edu.cn (M. Zhang), xuhui.lee@yale.edu (X. Lee).

https://doi.org/10.1016/j.agrformet.2021.108600
Received 6 May 2021; Received in revised form 31 July 2021; Accepted 3 August 2021
Available online 14 August 2021
0168-1923/© 2021 Elsevier B.V. All rights reserved.

natural ponds are in the range 100 to 700 g C $m^{-2}$ $y^{-1}$ through river inflow or in the range of 50 to 200 g C $m^{-2}$ $y^{-1}$ via in-situ production (Urban et al., 2005; Zhang et al., 2019; Kamula et al., 2020; Lu et al., 2021). According to a recent estimate by Yuan et al. (2019), aquaculture systems in the top 21 fish-producing countries emit a total amount of 6.04 ± 1.17 Tg $CH_4$ in 2014, equivalent to about 20 % of emission from global rice cultivation (30 Tg $CH_4$ $yr^{-1}$, Saunois et al., 2020). As Kosten et al. (2020) acknowledge, however, this estimate is preliminary and large uncertainties still exist due to lack of full-year observations and insufficient data to constrain the emission factor for different farming practices.

Aquaculture in China is the largest in the world, accounting for 60% of the global aquaculture production (FAO, 2020). This economic sector has been undergoing rapid expansion in recent years, with the national annual output nearly doubled in the last decade (FAO, 2020). More than half of the expansion has occurred via conversion of rice paddies to fishponds (Yuan et al., 2019, 2021). Since rice paddies are a large anthropogenic source of $CH_4$, an important question is whether this land conversion causes a net reduction in $CH_4$ emission. So far, the answer to this question has remained elusive. Using a year-long chamber flux measurement in the Yangtze River Delta (YRD) in eastern China, Yuan et al. (2019) found that conversion of rice paddies to crab ponds increased the annual $CH_4$ emission flux by 340% from 0.69 ± 0.02 μg $m^{-2}$ $s^{-1}$ to 3.05± 0.47 μg $m^{-2}$ $s^{-1}$. However, other chamber observations conducted in the same region showed 20% to 50% lower $CH_4$ fluxes from fish ponds than from rice paddies (Hu et al., 2016; Liu et al., 2016; Wu et al., 2018). This disparity is likely a result of different aquaculture farming practices. Some fish farmers deploy aerators to improve water quality. Aeration can reduce $CH_4$ emission by promoting $CH_4$ oxidation in the water column. According to Yuan et al. (2019), the high $CH_4$ flux in their study was attributed to the fact that their ponds were not equipped with aerators. Aerators were used in the studies by Hu et al. (2016) and Liu et al. (2016). Another potential contributor to the difference is dredging. Farmers occasionally dredge their pond prior to fish stocking to increase pond depth and to reduce the excessive nutrient accumulated over previous years. By removing the top sediment layer rich in organic matter, dredging can significantly reduce $CH_4$ production (Hu et al., 2016; Chen et al., 2021). It is worth noting that the ponds studied by Liu et al. (2016) and Hu et al. (2016) were dredged prior to the farming season but those studied by Yuan et al. (2019) had not been dredged since their conversion from rice paddies. It is not known which of the two practices (dredging or aeration) has a stronger effect on the $CH_4$ flux.

To date, the published data on aquaculture $CH_4$ emissions have been obtained either with flux chambers (FCs) or with the transfer coefficient method (Kosten et al., 2020). The transfer coefficient method combines observed $CH_4$ concentration in the water with a parameterization of the water-air transfer coefficient to determine the $CH_4$ diffusion flux to the atmosphere (Cole and Caraco, 1998). Even though it provides useful insights into biotic and abiotic controls on $CH_4$ production processes, this method is not suitable for quantifying the total $CH_4$ emission because it omits the $CH_4$ ebullition pathway. Kosten et al. (2020) argue that fluxes measured with FCs are biased low, and that the actual fluxes may be multiple times higher than the FC fluxes reported in the literature. One source of the bias is lack of FC observations during transitional times of draining and refilling when high emission fluxes are expected (Yang et al., 2017; Kosten et al., 2018). Additionally, site visits in FC studies tend to occur in daylight hours during which the flux may be lower than at night according to the diel flux pattern detected by eddy covariance in shallow lake systems (Podgrajsek et al., 2014; Zhang et al., 2019). Finally, large ebullition events can cause step-like changes in the $CH_4$ concentration in the chamber (Goodrich et al., 2011); such observations may be flagged as having poor data quality and be discarded.

Spatial variability in $CH_4$ emission is another methodological challenge confronting FC-based experimental studies. In a lake environment, changes in primary production (e.g., macrophyte vegetation abundance and algal growth), allochthonous river carbon input, lake morphology (e.g., lake area and standing water depth), water quality parameters (e.g., dissolved oxygen and pH) and sediment type can result in spatial variability in the $CH_4$ flux (Wang et al., 2006; Chen et al., 2009; Natchimuthu et al., 2015; Wik et al., 2016; Xiao et al., 2017; Loken et al., 2019; Denfeld et al., 2020). In an aquaculture system, management regimes can further amplify flux spatial variations. In a study of coastal shrimp ponds, Yang et al. (2019) reported that the $CH_4$ flux in the feeding zone is four to ten times greater than the flux observed in the aeration zone. In other aquaculture studies in the published literature, the flux values are typically based on FC observations replicated at 2 to 3 locations (e.g., Hu et al., 2016; Liu et al., 2016; Ma et al., 2018; Wu et al., 2018; Yang et al., 2019; Yuan et al., 2019; Yang et al., 2020; Yuan et al., 2021). The study by Yang et al. (2019) implies that a greater number of spatial replicates may be required to obtain an accurate whole-system $CH_4$ emission rate.

In this study, we deployed the eddy covariance method to measure the $CH_4$ flux of a fishpond complex in the YRD. The observation was made on a near-continuous basis for four years. To our best knowledge, this study represents the first EC application to an aquaculture ecosystem. Because the measured flux has relatively large footprints on the order of tens of meters, the EC method is less prone to errors arising from microscale spatial variability than the FC method. Another strength is that the EC method is unbiased over time (Baldocchi et al., 1988; Knox et al., 2019; Baldocchi, 2020), providing observation during normal periods as well as during episodic flux events and transitional times of pond management. Our goals were (1) to investigate the temporal dynamics of the $CH_4$ flux and the associated drivers at multiple timescales (from hours to years), (2) to constrain the component contributions to the whole-system flux by comparing the EC data with measurement made with inverse funnels and flux chambers, and (3) to synthesize the observed annual fluxes and the published emission data in relation to key farming practices. Ultimately, the results presented here may provide a basis for efforts to formulate management strategies for mitigating $CH_4$ emissions without compromising fish yield.

## 2. Methods

### 2.1. Site information

The present study was conducted in Anhui Province, in the YRD region, Eastern China (31° 58′ N, 118° 15′ E). This region is characterized by a subtropical monsoon climate, with local annual mean air temperature and rainfall of 15.8°C and 1087 mm from 1980 to 2019. The field experiment was carried out in four adjacent aquaculture ponds, labeled as C, D, E and F, from 2016 to 2019 (Fig. 1). These ponds (each about 0.7 ha or 110 m × 60 m in size) were situated in a landscape dominated by rice paddies and small irrigation ditches (Zhao et al., 2019b). They were converted in 1985 from rice cultivation and have never been dredged since then. Their banks were built with sediment excavated from the edge of the paddy fields. The difference in water level between these ponds and the adjacent rice paddies was 0.8 m to 1.8 m during the aquaculture period. The farmers used two species combinations typical of this region. In 2016, Ponds D and F were used to raise crayfish-small fry (C-S), and Ponds C and E to raise fish-clam (F-C). In 2017, Pond C was used for C-S, and Ponds D, E and F for F-C. In 2018 and 2019, all four ponds were used for F-C.

During the C-S cultivation phase, the pond was drained in late January. Ryegrass and barnyard grass were planted sparsely in early April to provide supplementary food and habitat for crayfish. The pond was filled with water in early May, and young crayfish were introduced into the pond at a stocking density of 30000 ind $ha^{-1}$ (350 kg $ha^{-1}$). The crayfish were fed mainly with commercial artificial diet and supplemented with corn seed, twice per day at 08:00 and 18:00. Harvesting of the crayfish occurred in mid-June. After that, small fries were introduced into the pond at a stocking density of about 210000 ind $ha^{-1}$ (210

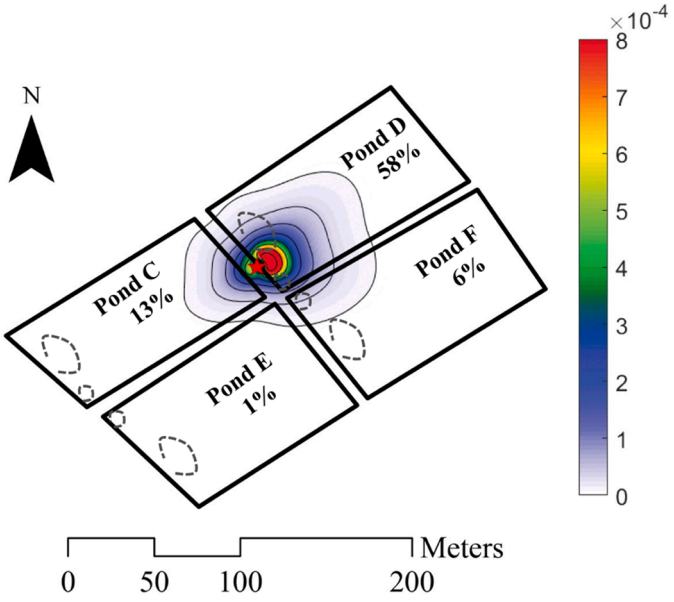


**Fig. 1.** Map showing the target ponds (Ponds C to F), EC measurement location (marked by the red star) and flux footprint for the EC system in 2018. Footprint contour lines are shown in intervals of 10% from 10% to 80%. The percent value in each panel is the source contribution from every pond in 2018. Grey dashed lines mark feeding zones.

kg ha$^{-1}$). Feeding (commercial artificial diet and soybean) were provided four times per day at 09:00, 11:00, 14:00 and 18:00. Harvesting of the small fry occurred in late January. The annual total inputs of soybean and commercial artificial diet were 418 kg ha$^{-1}$ and 9766 kg ha$^{-1}$ (both dry weight), respectively. The equivalent C input density was about 17 g C m$^{-2}$ y$^{-1}$ and 320 g C m$^{-2}$ y$^{-1}$, using a carbon content of soybean and artificial diet of 39.5% and 32.8%, respectively. The water depth was maintained at around 1.0 m from early May onward.

Species used for F-C polyculture included six fish species (*Grass carp, Aristichthys nobilis, Hypophthalmichthys molitrix, Mylopharyngodon piceus, Carassius auratus,* and *parabramis pekinensis*) mixing with clam. Young fish were introduced at a stocking density of 2100 kg ha$^{-1}$ in early February. They were fed with commercial artificial diet three times per day, at 09:30, 12:30, and 18:00. The annual total food input was 17440 kg ha$^{-1}$ (dry weight) or 570 g C m$^{-2}$ y$^{-1}$ from 2016 to 2018. In 2019, in order to improve the fish yield, more young fish were introduced with the annual total food input of 21630 kg ha$^{-1}$ or 710 g C m$^{-2}$ y$^{-1}$. In addition, chicken manure was applied in early February and late November to stimulate phytoplankton growth, at an annual total of 13950 kg ha$^{-1}$(wet weight). The C input via chicken manure was equivalent to 285 g C m$^{-2}$ y$^{-1}$, using a water content and carbon content of 40 % and 34%, respectively. The approximate feed zone positions are indicated in Fig. 1. The pond used for F-C cultivation was inundated all year round except for a short (seven days) harvest period in January or February, with an average water depth of around 1.8 m.

No aeration was deployed during the C-S cultivation phase. During the F-C cultivation phase, the pond was equipped with a surface impeller aerator. The aerator was activated daily between about 10 PM and 05 AM local time from August to October. In June and July, it was occasionally activated on rainy days and on days with low wind and overcast skies. (Aeration timing in June and July was not recorded.) Aerators were positioned at the center of the ponds.

During the F-C cultivation phase, the mean surface water (0 to 20 cm) dissolved oxygen (DO) concentration and pH in the water column averaged 8.95 mg L$^{-1}$ and 8.2 respectively. The water total phosphorus (TP) and total nitrogen (TN) concentrations averaged at 0.22 mg L$^{-1}$ and 3.58 mg L$^{-1}$, respectively. These measurements were made once a day during the four intensive field campaigns on ebullition in 2018 (Section 2.4). No water quality data were available for the C-S cultivation phase.

### 2.2. Eddy covariance flux measurement

The $CO_2$, $H_2O$ and $CH_4$ fluxes were measured with an EC system from 2016 to 2019. From January 7 to March 23, 2016, the system consisted of a three-dimensional sonic anemometer/thermometer (Model CSAT3A, Campbell Scientific Inc., Logan, Utah, USA) and an open-path $CO_2$/$H_2O$ infrared gas analyzer (model EC150, Campbell Scientific Inc.). On March 25, 2016, an open-path $CH_4$ gas analyzer (model LI-7700, LI-COR Inc., Lincoln, Nebraska, USA) was added to the system. The EC system was oriented towards the prevailing wind direction at an azimuthal angle of 40$^o$. The EC height was 1.8 m and 1.0 m above the water surface during the C-S and the F-C cultivation phase, respectively. Raw data were recorded at 10 Hz by a data logger (model CR3000, Campbell Scientific Inc.) for offline flux calculation. The two gas analyzers were calibrated every 6 to 12 months using ultra high-purity nitrogen as the zero-point reference and two standard gases for $CO_2$ gain correction (444 ppm and 501 ppm, uncertainty: 1.5%) and one standard gas for $CH_4$ gain correction (3.52 ppm, uncertainty: 1%). The observation was nearly continuous except for four periods due to power failure and LI-7700 equipment malfunction. They were June 1 to July 12, 2016, November 22 to December 22, 2016, July 21 to September 1, 2017, and February 1 to May 1, 2019.

The 10 Hz raw data were processed into 30-min fluxes using the Eddypro software (version 6.2.1; LI-COR Inc.). Imbedded in the software are the following numerical corrections. The time lags resulting from the separation between the anemometer and the analyzers were compensated with a cross-correlation maximum procedure for each 30-min averaging interval. A double coordinate rotation method was performed to force the mean vertical wind velocity to zero for each half-hour period (e.g., Tanner and Thurtell, 1969; Lee et al., 2004). The WPL density correction was applied to the measured gaseous fluxes (Webb et al., 1980). Spectroscopic effects of pressure, temperature, and water vapor fluctuations on $CH_4$ flux was removed with the method provided by McDermitt et al. (2011). High-frequency damping loss caused by sensor separation and path-length averaging was compensated following the frequency response method proposed by Moncrieff et al. (1997). On average, this frequency correction increased the flux of $CH_4$, $CO_2$ and $H_2O$ by 18%, 14% and 8%, respectively. In addition, a small spectroscopic effect on the $CO_2$ flux associated with the EC150 analyzer was corrected according to Helbig et al. (2016).

The EC measurement was screened for data quality. Observations interfered by power disruption, dirty optical window, and precipitation were discarded. The steady-state and the integral turbulence tests descirbed by Mauder and Foken (2004) were applied. Each 30-min observation was assigned a quality flag of 0 (best quality), 1 (good quality), or 2 (bad quality). Data with flag 2 were excluded from further analysis. Furthermore, the nighttime $CH_4$ flux was screened with the friction velocity ($u_*$) threshold method. The threshold was quantified with the REddyProc software (version 1.2.2) using the relationship between the nighttime $CO_2$ flux versus $u_*$ (Papale et al., 2006). At this site, the $u_*$ threshold among four years varies between 0.09 m s$^{-1}$ (2017) and 0.15 m s$^{-1}$ (2016). The threshold method increased the mean $CH_4$ flux slightly (by 3 %). The total number of valid half-hourly observations is 21191 for the $CH_4$ flux and 44937 for the $CO_2$ flux, representing 30% and 64% of the half-hourly periods from 2016 to 2019, respectively.

Gap-filling was performed to obtain daily, monthly and annual $CH_4$ and $CO_2$ fluxes. For $CH_4$, the daily mean flux was first calculated as the mean of all valid half-hourly observations for days with half-hourly data coverage higher than 60%. For other days, the daily flux was filled with the exponential relationship between the observed daily flux and water temperature at a water depth of 20 cm ($F = a\, e^{b\, T_w}$, fitting equation shown in Fig. 6b). The flux temperature sensitivity or $Q_{10}$ is obtained from the fitting parameter $b$ as $Q_{10} = e^{10b}$. Monthly and annual fluxes were based on the gap-filled daily values.

For $CO_2$, the nighttime flux data were first filtered with $u_*$. The half-hourly $CO_2$ flux data gaps (resulting from $u_*$ screening and missing observations) were filled using the REddyProc software. The main input variables include half-hourly EC $CO_2$ flux, friction velocity, global radiation, air temperature, and vapor pressure deficit. The software uses a combination of three gap-filling methods, including look-up tables, mean diurnal course, and marginal distribution sampling. The uncertainty of the annual $CO_2$ flux was estimated by the difference between maximum and minimum values derived from different quantiles (5th, 50th, 95th) of the $u_*$ threshold estimate (Morgenstern et al., 2004; Zhao et al., 2019a).

### 2.3. Floating chamber measurement

A floating flux chamber system was deployed during three intensive field campaigns, from January 4 to January 19, May 3 to May 13, and July 24 to August 5, 2019, to quantify spatial variation of the $CH_4$ flux and relative flux contributions via the ebullition and the diffusion pathway. Four chambers (32 cm in diameter and 40 cm in height and made of polypropylene) were placed at four spots in a 30 m-long linear transect between the feeding zone near the southwest edge of Pond D and the aerator zone located at the center of the pond. The chambers were suspended above the water surface by floats. The chamber measurement was made for five cycles a day between 08:30 AM and 06:00 PM local time. During a measurement cycle, one chamber was lowered, by partially deflating its float, to the water column with its bottom to a depth of 0.05 m for a length of 15 min. A small air stream from the partially submerged chamber was drawn through a closed loop at a flow rate of 1 L $min^{-1}$ to a $CH_4/CO_2/H_2O$ analyzer (model 915-0011-CUSTOM, Los Gatos Research Ltd., San Jose, California, USA) for detection of the $CH_4$ concentration. The process was repeated sequentially for all the four chambers. A complete measurement cycle was about 120 min. The sampling rate of the chamber headspace $CH_4$ concentration was 1 Hz. The sampling Teflon tube (tube inner diameter, 0.32 cm) was 10 m long (one-way).

The chamber flux was calculated with the gas concentration change in the chamber over time (the concentration difference at the beginning and end of measurement period) and the chamber base area (Schubert et al., 2012). The first 120 s after chamber closure were discarded from the flux calculation. Because the concentration was recorded at a high frequency, the chamber observation could be separated into diffusive flux and episodic ebullition events. According to Goodrich et al. (2011) and Xiao et al. (2014), an ebullition event is defined by a sharp step increase in the $CH_4$ concentration over time and a diffusion event corresponds to a gradual and linear rise over time. Using their method, we calculated the diffusion and the ebullition contributions to the total chamber flux for each measurement cycle.

### 2.4. Ebullition measurement

A total of 10 bubble traps were used in Pond D and Pond E (Fig. 1) to measure the ebullition flux during eight field campaigns in 2016, 2017 and 2018, each lasting about 12 days (Fig. 2). Their positions are indicated in Fig. 13 below (Section 4.1). These traps were positioned within 1 m from the edge except for two traps (labeled as D5 and E5) which were at a distance of about 5 m from the edge. The trap was an inverted funnel (IF: collection area 0.071 $m^2$) with a clear tube (0.30 m tall, inner diameter: 0.20 m, PVC) attached to the funnel neck. The other end of the tube was sealed with a three-way valve. Each measurement lasted about 24 h, from 07:00 AM to 07:00 AM the next day or 03:00 PM to 03:00 PM the next day. At the end of the measurement, the total volume of the gas accumulated in the tube was recorded and a gas sample was collected through the three-way valve with an airtight syringe. The air samples were immediately brought back to the laboratory for analysis of the $CH_4$ concentration by gas chromatograph (Model: GC7890B, Agilent Technologies Inc., Santa Clara, CA, USA). The ebullition flux was determined from the total amount of $CH_4$ collected, collection time and collection area (Wik et al., 2013).

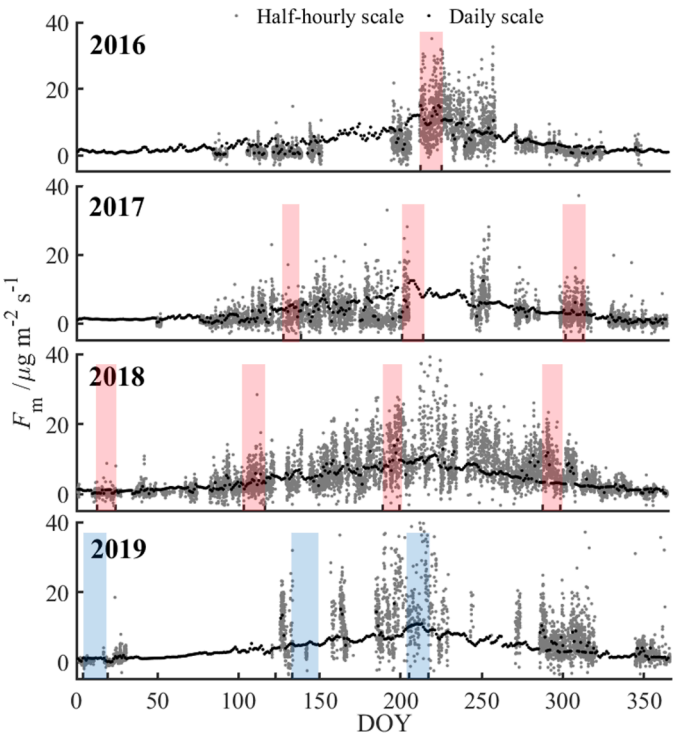


**Fig. 2.** Temporal variations of $CH_4$ flux across different time scales. Red shadows indicate inverted funnel observation periods. Blue shadows mark periods of floating chamber observation.

### 2.5. Supporting measurements

In parallel to the EC measurement, air temperature and relative humidity were observed using a temperature/humidity probe (Model HMP155, Vaisala Inc., Helsinki, Finland). Wind speed and wind direction were measured by an anemometer and a wind vane (Model 05103, R M Young Company, Traverse City, Michigan, USA). Water temperature at the depths of 20, 50, 80 cm, and sediment temperature were measured with a chain of temperature probes (Model 109-L, Campbell Scientific Inc.). The four components of the surface radiation balance were measured with four-way net radiometer (model CNR4, Kipp&Zonen B.V., Delft, the Netherlands).

### 2.6. Footprint modeling

A two-dimensional flux footprint model proposed by Kljun et al. (2015) was employed to quantify the contribution from target ponds to the measured fluxes. The main input variables were provided by our measurement systems, including measurement height, surface roughness, the Obukhov length, friction velocity, the standard deviation of the cross-wind component, and wind speed and direction. The boundary layer height required by the model was provided by the Global Data Assimilation System of the U.S. National Oceanic and Atmospheric Administration (https://ready.arl.noaa.gov/gdas1.php). The calculation was performed for each half-hourly observation and the result was aggregated to produce a footprint climatology for each year.

### 2.7. Data analysis

Single-variable regression was performed to investigate the relationships between annual $CH_4$ and $CO_2$ flux with carbon input, between the $CH_4$ fluxes observed with the three methods, and between the

$CH_4$ flux and temperatures. A student t-test was performed to evaluate the effect of management practices (aeration period versus non-aeration period, drainage period versus flooding period, dredging site versus non-dredging site, aeration site versus non-aeration site) as well as among different observation methods. A two-way analysis of variance (ANOVA) was conducted to examine the effects of dredging and aeration on the $CH_4$ flux, using data found in the published literature.

## 3. Results

### 3.1. Climatology of the eddy flux footprint

An example of footprint climatology is given in Fig. 1 for 2018. The footprint distributions for the other three years are broadly similar. The flux footprint was mostly confined to the four target ponds. In 2018, these ponds contributed to 78% the observed flux, with the largest contributor being Pond D (58%). The maximal contribution for each 30-min averaging period occurred at a distance of 4 m to 10 m from the flux tower, depending on stability. The total contributions from the four ponds were also sensitive to stability, varying from 75% in unstable to 70% in neutral and 50% in stable conditions.

The annual carbon input and fish harvest in each pond was weighted by their annual footprint contributions to produce a four-pond mean values for comparison with the annual mean eddy $CH_4$ and $CO_2$ fluxes. The annual footprint-weighted C input was 4200, 7300, 8570 and 9940 kg C $ha^{-1}$ in 2016, 2017, 2018, and 2019, respectively. In comparison, the carbon output in the form of fish harvest was 500, 1000, 1500 and 2290 kg C $ha^{-1}$, respectively, representing a small part of the carbon input from feed and fertilizer.

### 3.2. Temporal patterns of the EC $CH_4$ and $CO_2$ fluxes

The aquaculture ponds in the present study were a $CH_4$ source of emission to the atmosphere throughout the experimental period (Fig. 2). The daily flux ranged from 0.1 to 16.7 μg $m^{-2}$ $s^{-1}$, with an average value of 4.10 ± 3.08 μg $m^{-2}$ $s^{-1}$ during the four-year observation period. The $CH_4$ flux displayed strong seasonal changes in all the years, with much higher value in the summer (7.84 ± 2.56 μg $m^{-2}$ $s^{-1}$; June – August) than in the winter (1.21± 0.54 μg $m^{-2}$ $s^{-1}$; December – February). In addition to seasonal differences, some inter-annual differences were observed. The annual gap-filled flux was 1230, 1140, 1400, and 1390 kg $CH_4$ $ha^{-1}$ in 2016, 2017, 2018, and 2019, respectively. These annual values were weakly correlated with the annual organic C input (Fig. 4a). About 50% of the annual total emissions occurred during high-temperature summer season (June – August). In addition, as depicted in Fig. 2, high $CH_4$ emission spikes (flux > 20 μg $m^{-2}$ $s^{-1}$) were frequently observed at the half-hourly scale, possibly caused by ebullition events.

From March 24 to May 08 2016, Ponds D and F were drained, while Ponds C and E had a normal water depth of 1.5 m. This transitional period provided an opportunity to examine the effect of drainage on the methane flux. Fig. 5 shows the time series of half-hourly data collected during this period. There was no field $CH_4$ flux observation before March 2016. These observations were divided into three categories, those with footprint contribution from Ponds D and F exceeding 50%, those with contribution from Ponds C and E exceeding 50%, and those with mixed footprint. The mean $CH_4$ flux from the drained ponds was 0.75 ± 0.86 μg $m^{-2}$ $s^{-1}$ (n = 401). In comparison, the mean flux (1.25 ± 1.45 μg $m^{-2}$ $s^{-1}$, n = 310) from the wet ponds was significantly higher ($p < 0.05$).

The daily $CO_2$ flux displayed relatively large random variations (Fig. 3). The 25- and 75-percentile daily flux values are -0.019 mg $m^{-2}$ $s^{-1}$ and 0.029 mg $m^{-2}$ $s^{-1}$, respectively. In 2016, the monthly mean flux was negative in the summer indicating uptake of $CO_2$ from the atmosphere and was slightly positive in the winter indicating $CO_2$ release. We attribute the summer uptake to the growth of ryegrass and barnyard grass in Ponds D and F (Fig. 1) in the C-S cultivation phase in 2016.

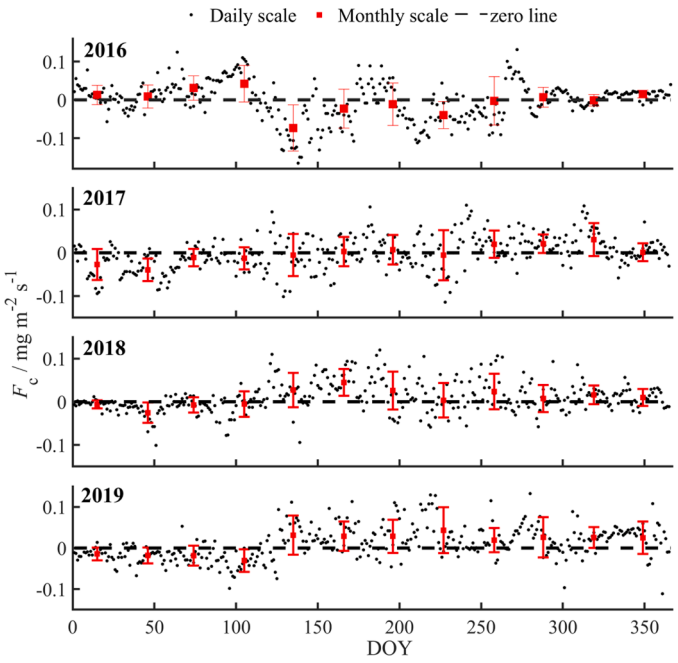


**Fig. 3.** Temporal variations of $CO_2$ flux across different time scales.

According to Sentinel-2 satellite imagery, the NDVI of these two ponds was 0.20 in the summer of 2016, which is higher than in other summers (0.10). No obvious uptake signal was detected in the other three years. In 2018 and 2019, the monthly flux was generally more positive in the summer than in the other seasons, which is indicative of enhanced organic matter decomposition due to feeding and chicken manure application. The annual mean flux ranged from -0.0008 mg C $m^{-2}$ $s^{-1}$ (-250 kg C $ha^{-1}$ $y^{-1}$; 2016) to 0.0034 mg C $m^{-2}$ $s^{-1}$ (1080 kg C $ha^{-1}$ $y^{-1}$; 2019), and was positively correlated with the annual organic C input (Fig. 4b).

### 3.3. Dependence of the EC $CH_4$ flux on temperature

The EC $CH_4$ flux was positively correlated with water temperature at the 20-cm depth, at half-hourly (Fig. 6, panel a), daily (panel b) and monthly (panel c) scale. The relationship was exponential, with nearly indentical coefficient of the exponent or a $Q_{10}$ value (2.1 to 2.2) across these three time scales. At the daily time scale, the exponential fit with the 20-cm water temperature yields a slightly higher $R^2$ value (0.42) than the fit with air temperature ($R^2$ = 0.34) or with the sediment temperature ($R^2$ = 0.41), implying that the $CH_4$ emission rate was more

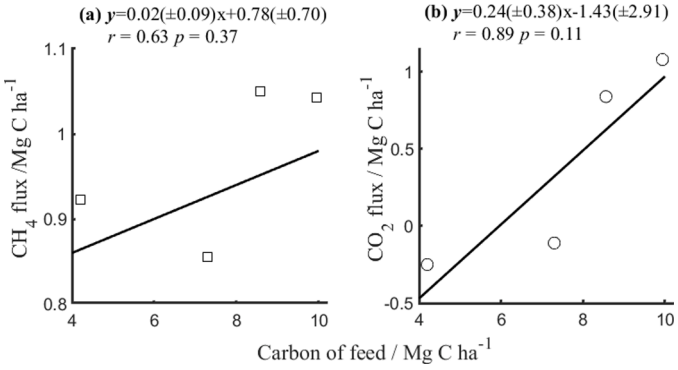


**Fig. 4.** Dependence of annual $CH_4$ flux and $CO_2$ flux on annual carbon input via feed material and fertilizer application. Also shown are regression equation, linear correlation ($r$) and significance ($p$). Parameter bounds on the regression coefficients are 95% confidence intervals.

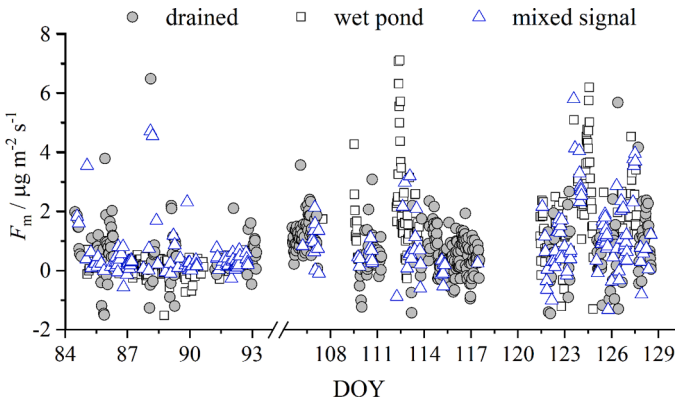


**Fig. 5.** Time series of half-hourly $CH_4$ flux collected during periods when footprint was dominated by the drained pond (gray circles), by the wet ponds (black squares) and by mixing signals (blue triangles).

dependent on the variation of water temperature. At the monthly time scale, the exponential fit with the water temperature can explain nearly 60% of the monthly $CH_4$ flux variations across the four observational years.

### 3.4. Effect of aeration on the EC $CH_4$ flux

The effect of aeration on the $CH_4$ flux was evaluated through comparison between aeration periods and non-aeration periods. Fig. 7 shows the half-hourly flux data collected during aeration periods (between 10:00 PM and 05:00 AM the next day, August to October) and non-aeration periods (between 05:30 AM and 09:30 PM in other months) as a function of water temperature. The mean value with aeration was $8.82 \pm 5.75$ μg m$^{-2}$ s$^{-1}$ (n = 320) in 2018 and $6.94 \pm 6.33$ μg m$^{-2}$ s$^{-1}$ (n = 171) in 2019. The aeration occurred in a broad temperature range of 17 °C to 36 °C. The mean flux measured in this temperature range without aeration was lower, at $6.38 \pm 5.14$ μg m$^{-2}$ s$^{-1}$ (n = 635) in 2018 but was higher, at $10.58 \pm 7.09$ μg m$^{-2}$ s$^{-1}$ (n =225) in 2019. The difference between the mean with and without aeration was statistically significant ($p < 0.05$) in both years.

### 3.5. Comparison of the EC, FC and IF methods

Fig. 8 is a comparison of the EC and FC $CH_4$ flux data. A total of 39 spatially replicated observations were made with the FC method. The two fluxes are significantly correlated ($r = 0.33$, $p < 0.05$), but a systematic difference is evident. The mean EC flux during the FC observational periods was $12.1 \pm 8.5$ μg m$^{-2}$ s$^{-1}$, while the mean FC flux was much higher at $24.8 \pm 18.3$ μg m$^{-2}$ s$^{-1}$. The large FC standard deviation was attributed to one chamber with an anomalously high flux in the spring and summer (section 4.1). If this chamber was excluded from the comparison, the data based on the remaining three chambers show the overall mean value was $10.3 \pm 8.6$ μg m$^{-2}$ s$^{-1}$, agreeing reasonably well with the mean EC flux.

Fig. 9 is a comparison of the ebullition flux measured with the IF method and the EC flux of the corresponding periods. Once again, although the two fluxes were weakly correlated ($r = 0.24$, $p = 0.14$, n = 41), a large difference was found. The mean EC flux was $6.53 \pm 4.45$ μg

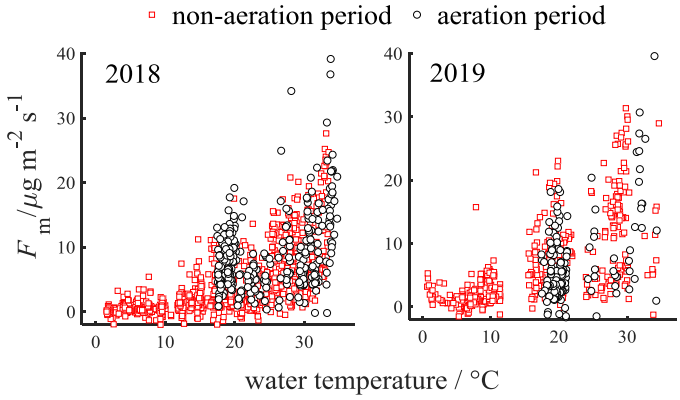


**Fig. 7.** Dependence of $CH_4$ flux ($F_m$ on water temperature during aeration periods (black circles) and non-aeration periods (red squares).

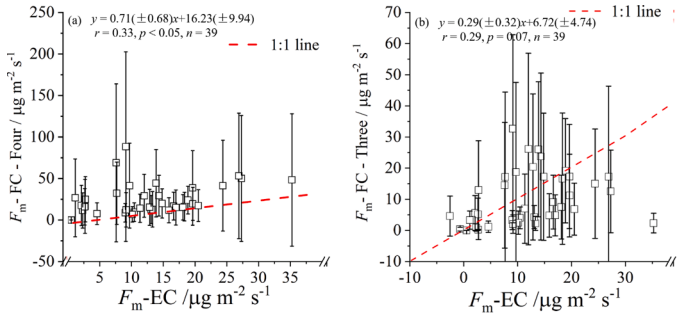


**Fig. 8.** Comparison of $CH_4$ flux obtained with the flux chamber method ($F_m$_FC) and the flux obtained with the eddy covariance method ($F_m$_EC). a: chamber flux is average of four spatial replicates. b: chamber flux is average of three spatial replicates. Error bars indicate one standard deviation of spatial replicates.

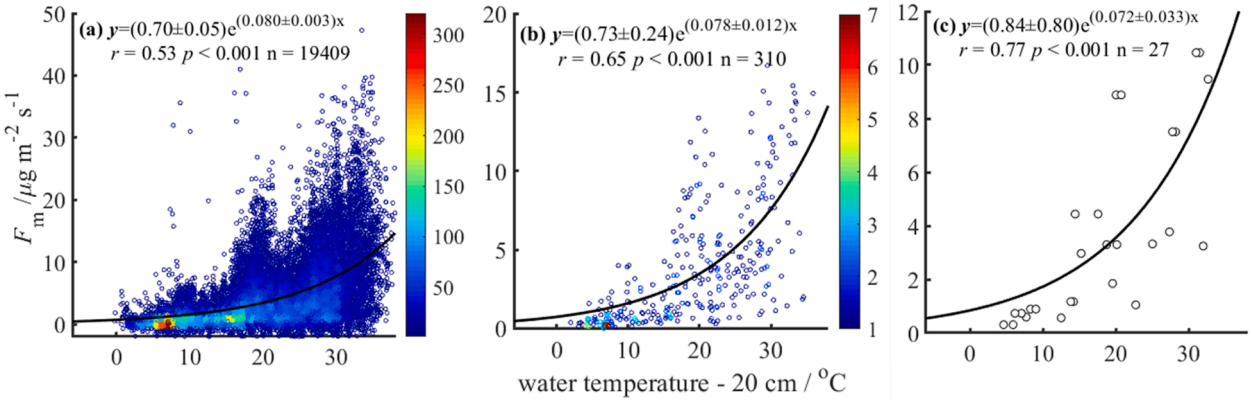


**Fig. 6.** Relationships between $CH_4$ flux ($F_m$) and water temperature at the 20-cm depth based on half-hourly (a), daily (b), and monthly scale (c). Also shown are regression equation, linear correlation ($r$), significance ($p$), and valid data ($n$). Parameter bounds on the regression coefficients are 95% confidence intervals. Color indicates data density.

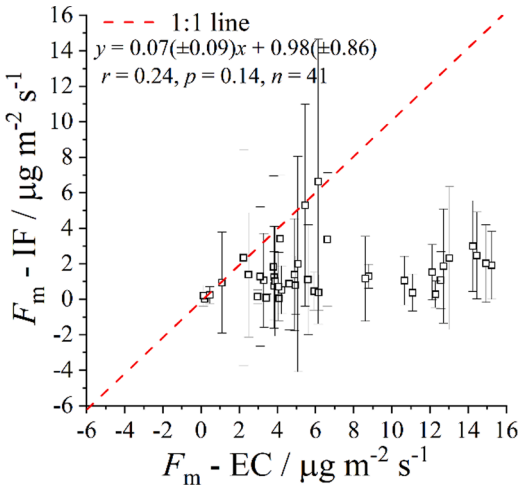


**Fig. 9.** Comparison of the $CH_4$ flux obtained with the inverted funnel method ($F_m$_IF) and that with the eddy covariance method ($F_m$_EC). Error bars indicate one standard deviation of ten spatial replicates.

$m^{-2}$ $s^{-1}$, while the mean IF flux was 80% lower, at 1.45 ± 1.37 μg $m^{-2}$ $s^{-1}$. The low IF flux may have been caused by bias sampling. The IFs were positioned near the edge of these ponds (Fig. 13 below) to facilitate sample retrieval. It appears that these locations experienced lower bubble formation than locations further away from the edge. As explained in Section 2.1, sediment at the edge was excavated to build bands when these ponds were first converted from rice cultivation. It is possible that owing to this disturbance, substrate near the pond edges had lower organic carbon levels than in other parts of the ponds.

### 3.6. Ebullition versus diffusion

We partitioned the chamber flux into the ebullition and the diffusion components with the high-frequency (1 Hz) $CH_4$ concentration time series measured inside the chamber, using the method described by Goodrich et al. (2011). The regression slope (mean ±1 standard deviation) of the ebullition flux versus the total flux was 0.70 ± 0.04, indicating an average of 70% ebullition and 30% diffusion contribution to the total $CH_4$ flux (Fig. 10a). The ebullition ratio shows some dependence on temperature, with lower ratios at higher temperatures (Fig. 10b). Two chamber observations made in the winter displayed

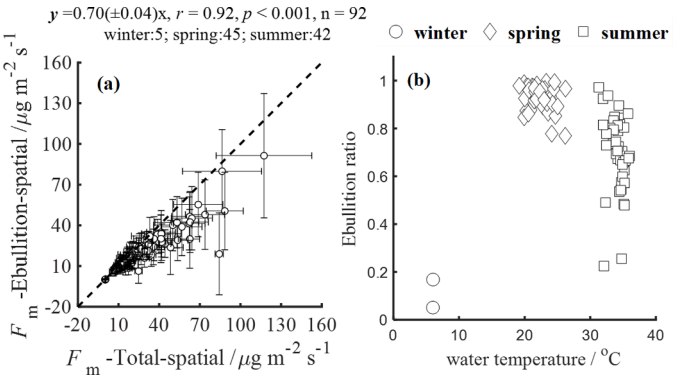


**Fig. 10.** (a) Comparison of the $CH_4$ total flux and ebullition flux measured by FC method. The error bars on the x and y axes represent standard error of $CH_4$ total flux and ebullition flux, respectively. Here FC observed results were averaged of four individual chamber observations. Also shown are regression equation, linear correlation ($r$), significance ($p$), and valid data ($n$). Parameter bounds on the regression coefficients are 95% confidence intervals. (b) Dependence of ebullition ratio on the 20-cm water temperature. Different symbols represent observations in different seasons.

extremely low ebullition ratios, which may have been related to the difficulty of the Goodrich et al.'s method in separating the diffusion and the ebullition contributions when the flux signal was weak (about 0.18 μg $m^{-2}$ $s^{-1}$). The mean ebullition ratio reported here is higher than most of the results given by a survey of global lake studies showing a range from 40% to 60% (Bastviken et al., 2004). The few published studies on aquaculture ponds also show higher ebullition ratios (80% to 90%; Yang et al., 2020; Yuan et al., 2021) than found for natural waters.

### 3.7. Annual carbon budget

Fig. 11 presents the carbon budget of the aquaculture ponds. On average, the annual C input via feeding and chicken manure application was 7.5 ± 2.5 Mg C $ha^{-1}$. The amount of carbon in fish harvest was 1.3 ± 0.8 Mg C $ha^{-1}$. The rate of sediment C accumulation, computed as a residual of the other C budget terms, was 4.8 ± 2.6 Mg C $ha^{-1}$. On the whole, these fishponds acted as a carbon source to the atmosphere. Averaged over the four-year period, about 70% (0.97 ± 0.10 Mg C $ha^{-1}$) of the C escaped to the atmosphere occurred in the form of $CH_4$ or twice as much as in the form of $CO_2$ (0.38 ± 0.66 Mg C $ha^{-1}$). The annual mean $CO_2$ flux ranged from -250 (±140) kg C $ha^{-1}$ $y^{-1}$ (2016) to 1080 (±14) kg C $ha^{-1}$ $y^{-1}$ (2019), and was positively correlated with the annual organic C input (Fig. 4b, linear correlation: $r$ = 0.89, $p$ = 0.11). The correlation between the annual $CH_4$ flux and the C input was weaker ($r$ = 0.63, $p$ = 0.37).

## 4. Discussion

### 4.1. $CH_4$ flux spatial variability

A number of studies have shown that $CH_4$ flux vary significantly in space in lake ecosystems (e.g., Wang et al., 2006; Chen et al., 2009; Wik et al., 2016; Xiao et al., 2017; Loken et al., 2019; Denfeld et al., 2020). Large spatial variability was also evident in this study based on the FC and IF observations. The FC $CH_4$ flux spanned two orders of magnitude ranging from 0.7 ± 1.0 μg $m^{-2}$ $s^{-1}$ to 111.8 ± 71.1 μg $m^{-2}$ $s^{-1}$ in the summer (Fig. 12c) and from 0.2 ± 0.2 μg $m^{-2}$ $s^{-1}$ to 43.5 ± 18.6 μg $m^{-2}$ $s^{-1}$ in the spring (Fig. 12b), along short linear transects of 30 m in

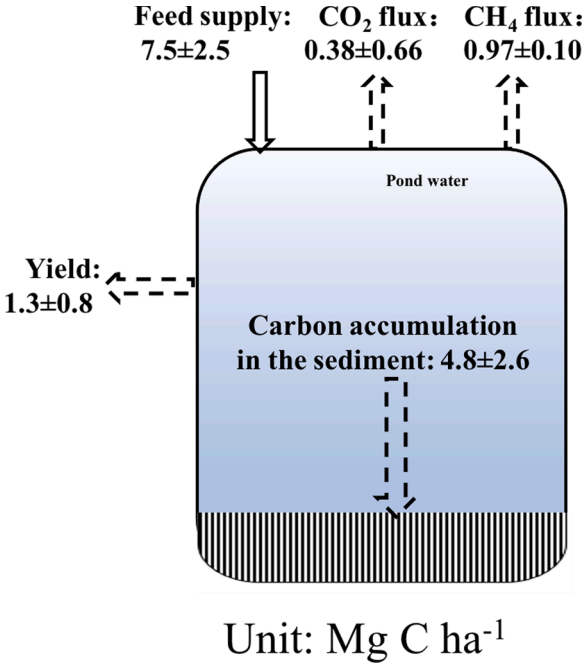


**Fig. 11.** Carbon budget of the aquaculture ponds (mean ± 1 standard deviation of inter-annual variations).

length. The $CH_4$ ebullition flux obtained with IFs also showed large spatial heterogeneity, ranging from 0.1 ± 0.4 μg $m^{-2}$ $s^{-1}$ to 5.5 ± 5.5 μg $m^{-2}$ $s^{-1}$ (Fig. 13). A study of $CH_4$ emission in mariculture ponds reveals spatial variations along gradients of management regimes, with the highest diffusion $CH_4$ flux occurring in the feeding zone (7.51 ± 1.47 μg $m^{-2}$ $s^{-1}$), followed by the nearshore zone (1.51 ± 0.22 μg $m^{-2}$ $s^{-1}$) and the aeration zone (0.84 ± 0.13 μg $m^{-2}$ $s^{-1}$; Yang et al., 2019). We did not have enough spatial replicates to systematically investigate the effects of feeding and aeration, but the high chamber flux at location D2 in the summer (Fig. 12c, pond D) and the high ebullition flux at location E2 (Fig. 13, pond E) were in line with Yang et al.'s results because these two measurement locations were within the feeding and fertilizer application zones.

The flux spatial variability is a factor contributing to the lack of agreement between the FCs and the EC $CH_4$ flux, especially in ecosystems with strong spatial heterogeneity (Schubert et al., 2012; Knox et al., 2019). In studies of rice paddies (Werle,1999; Werle and Korman, 2001; Meijide et al., 2011; Chaichana et al., 2018; Reba et al., 2020), the $CH_4$ flux measured with chambers is 30% to 95% higher than the flux measured with the EC method. In field experiments in Lake Wohlen, Switzerland, and Lake Kuivajärvi, Finland, considerable differences in $CH_4$ emission were found, with chamber flux about two times higher than that obtained with EC measurements (Eugster et al., 2011; Erkkilä et al., 2018). In this study, the mean chamber flux (24.8 ± 18.3 μg $m^{-2}$ $s^{-1}$) was twice as high as the EC flux (12.1 ± 8.5 μg $m^{-2}$ $s^{-1}$) observed in the same measurement periods (Fig. 8a) when equal weight was given to each of the four chamber locations. However, a footprint analysis for the

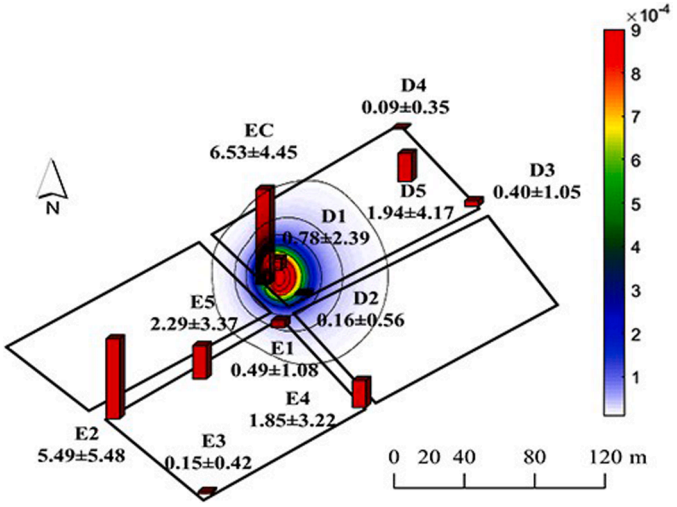


**Fig. 13.** Spatial pattern of the mean $CH_4$ flux measured with the IF method. Also shown are the EC mean value and footprint climatology during all IF observation periods.

FCs observation periods revealed that the highest $CH_4$ emission spot (D3 in the spring and D2 in the summer, Fig. 12b and c) was located near the outer edge of the average footprint. In other words, a simple arithmetic mean of the four FC observations would give this hot spot too much

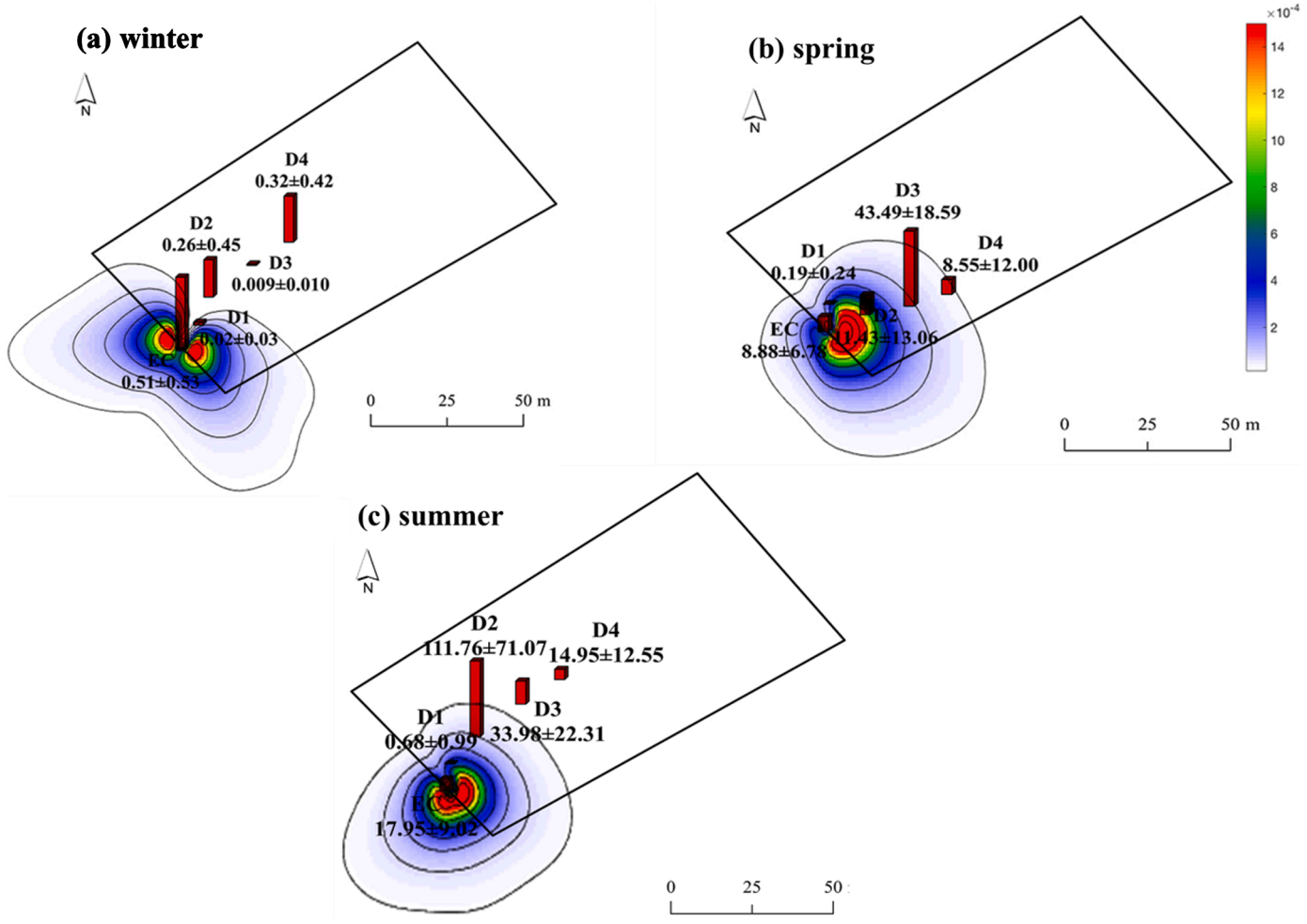


**Fig. 12.** Spatial pattern of $CH_4$ flux measured with the FC method in (a) winter, (b) spring and (c) summer. Also shown are the EC mean value and footprint climatology during the FC observation periods.

weight, leading to a substantial overestimation in comparison with the EC result.

It is helpful to point out that the annual mean footprint is much broader (Fig. 1) than that the footprint for FC measurement periods because the FC measurement occurred in mostly unstable atmospheric conditions. It is known that the EC flux footprint is much smaller under these conditions than under neutral and stable conditions (Tuovinen et al., 2019). Although the EC observation may have under-sampled the emission hotspot in the feeding zone in Pond D during the FC periods, the under-sampling was less of a problem when averaged over the year.

### 4.2. Uncertainties of the EC $CH_4$ flux

The EC $CH_4$ fluxes are affected by systematic and random errors, mainly high frequency loss, footprint contamination and data gaps (Knox et al., 2019; Kim et al., 2020). Previously, using a subset of the EC data, we showed that the high frequency loss due to a combination of the low EC instrument height and a long optical path of the $CH_4$ analyzer was about 18% (Zhao et al., 2019b). In the data presented above, the high frequency loss was corrected using the method proposed by Moncrieff et al. (1997). The EC flux after this correction agreed well with the flux obtained independently with the flux-gradient method (Zhao et al., 2019b).

Footprint contamination is another important source of uncertainty for the EC flux observation, especially at sites with limited fetch such as ours. Despite the low measurement height, our EC footprint still extended beyond the boundary of the target ponds. When averaged over the four measurement years, about 25 % of the flux was attributed to sources outside the pond complex according to the footprint model of Kljun et al. (2015). These outside sources were mainly rice paddies. A survey of $CH_4$ flux observations made in rice paddies in the Yangtze River Delta region reveals a mean annual flux of 0.69 ± 0.02 μg $m^{-2}$ $s^{-1}$ (mean ± 1 standard deviation; Yuan et al., 2019), which is significantly lower than the mean flux of 4.10 ± 3.08 μg $m^{-2}$ $s^{-1}$ reported above. In other words, it is likely that our observed flux was biased low due to footprint contamination. A simple two-source calculation, using 25% and 75% footprint contributions from the rice paddies and the fishponds, respectively, suggests that the bias error is on the order of 20%.

Finally, gap-filling can introduce uncertainty to the annual $CH_4$ flux. Similar to the studies by Xiao et al. (2017) and Zhang et al. (2019), here data gaps were filled with an exponential regression model with water temperature ($T_w$) as $F = a\, e^{b\, T_w}$. A simple Monte-Carlo simulation was conducted to estimate the flux error associated with this procedure. This simulation consisted of 10000 ensemble members. In each ensemble, the two coefficients of the regression model were drawn randomly from normal distributions whose standard deviations, taken as ½ of the 95 % confidence bounds, were 0.006 °$C^{-1}$ for exponent $b$ and 0.12 μg $m^{-2}$ $s^{-1}$ for coefficient $a$ (Fig. 6 b), and the gaps were filled with the model with the chosen coefficient values. The standard deviation of the annual mean flux based on the 10000 ensemble members is 15 g C $m^{-2}$ $yr^{-1}$ when averaged over the four years period. The uncertainty due to gap-filling was higher than the median uncertainty value of ±1.0 g C $m^{-2}$ $yr^{-1}$ of global synthesis results derived from EC $CH_4$ tower data from 60 sites (Knox et al., 2019).

### 4.3. Comparison with $CH_4$ emission fluxes published in the literature

The annual $CH_4$ flux reported here 97 ± 10 g C $m^{-2}$ $yr^{-1}$ (mean ± 1 standard deviation of interannual variations) throughout the experimental period is near the high end of the flux values reported in the literature for upland ecosystems, inland waters and wetlands. A recent synthesis study by Knox et al. (2019), which includes EC measurements at 60 sites, shows that the annual $CH_4$ flux ranges from -0.2 ± 0.02 g C $m^{-2}$ $yr^{-1}$ for an upland forest to 114.9 ± 13.4 g C $m^{-2}$ $yr^{-1}$ for a freshwater marsh (Fig. 14a). The $CH_4$ flux reported here was approximately six to seven times higher than the median annual flux from rice paddies (12.6 ± 1.6 g C $m^{-2}$ $yr^{-1}$) in this synthesis as well as the IPCC default emission factor of 15 g C $m^{-2}$ $yr^{-1}$ for rice paddies (Sass, 2003). When examined individually, only one site in Knox's data group – a highly productive estuarine freshwater marsh in Northern Ohio, USA – exhibits a higher annual flux (114.9 g C $m^{-2}$ $yr^{-1}$, Rey-Sanchez et al., 2018) than ours. The high annual $CH_4$ emission from the present study was primarily attributed to the high annual organic carbon input. The annual footprint-weighted organic carbon input was 750 ± 250 g C $m^{-2}$ $y^{-1}$, which is 3 to 15 times higher than a typical in-situ production rate (50 to 200 g C $m^{-2}$ $y^{-1}$) in lakes and ponds (Urban et al., 2005; Zhang et al., 2019). Furthermore, organic compounds in fish feed and feces, having high starch and protein contents, are more easily decomposed into methanogenic substrates than plant residues such stems and roots (Yuan et al., 2021). Because the ponds in the present study have never been dredged, old organic carbon accumulated in the sediment in years prior to the experiment may also have contributed to the high $CH_4$ flux. According to the carbon budget calculation, the rate of C accumulation in the sediment was about 480 g C $m^{-2}$ $yr^{-1}$.

The $CH_4$ flux shown here is higher than the median of flux values reported previously for other freshwater aquaculture ponds (Fig. 14b, Table S1). The difference is statistically significant at $p < 0.05$ for the annual flux and at $p < 0.05$ for the mean flux over the aquaculture period (from April to October; one-sample $t$ test). Of the eleven freshwater aquaculture pond studies cited here, ten are located in subtropical climate conditions similar to this study.

To investigate the effect of aquaculture farming practice on the $CH_4$ flux, we first divided the data in Fig. 14b into two groups, one with dredging and the other without dredging (Fig. 15, panel a and b). The results show that the annual $CH_4$ flux in the ponds with dredging (0.17 ± 0.07 μg $m^{-2}$ $s^{-1}$) was much lower than in the ponds without dredging (2.32 ±1.62 μg $m^{-2}$ $s^{-1}$), the difference being statistically significant at $p < 0.05$ (Fig. 15 panel a). The difference between the two data groups is also statistically significant for the aquaculture period ($p < 0.05$; Fig. 15 panel b). Next, we divided the data further. In the group without dredging, four studies deployed aeration and eight did not at the annual time scale, and no significant difference was found between the ponds with aeration and those without ($p = 0.08$; Fig. 15 panel c). Similarly, aeration had no significant impact on the mean flux during the aquaculture period (Fig. 15 panel d, $p = 0.93$). Finally, a two-way ANOVA was performed using the data in Fig. 14b to further examine the effect of dredging and aeration on the mean $CH_4$ flux. The results show that during the aquaculture period dredging produce a significant impact on the mean $CH_4$ flux ($p < 0.05$), and the effect of aeration on the $CH_4$ flux is not significant ($p = 0.22$). This data synthesis suggests that dredging plays a larger role than aeration in reducing $CH_4$ emission from freshwater aquaculture ponds.

## 5. Conclusion

The annual $CH_4$ flux of our fish ponds ranged from 86 to 105 g C $m^{-2}$ $yr^{-1}$, with a four-year mean value of 97 g C $m^{-2}$ $yr^{-1}$. For comparison, the median annual flux value reported previously for other freshwater aquaculture ponds under similar climate conditions is only 30 g C $m^{-2}$ $yr^{-1}$. An ANOVA analysis of the published results reveals much lower $CH_4$ emissions in ponds with dredging than those without dredging. Estimates of regional and global aquaculture $CH_4$ emission should take this land use legacy into account, in addition to considering aeration status. Manipulation field studies, in which intact ponds serve as control and dredged ponds as manipulation, will be helpful to further quantify the role of dredging on the $CH_4$ emission.

The $CH_4$ flux showed large spatial variations in the range of 0.7 to 112 μg $m^{-2}$ $s^{-1}$ in the summer according to the floating chamber measurement. Large spatial variations were also observed in the ebullition flux with the inverted funnel method (0.1 to 5.5 μg $m^{-2}$ $s^{-1}$in the summer). Future research should aim to quantify the mechanisms that drive these spatial variations to better inform experimental designs for

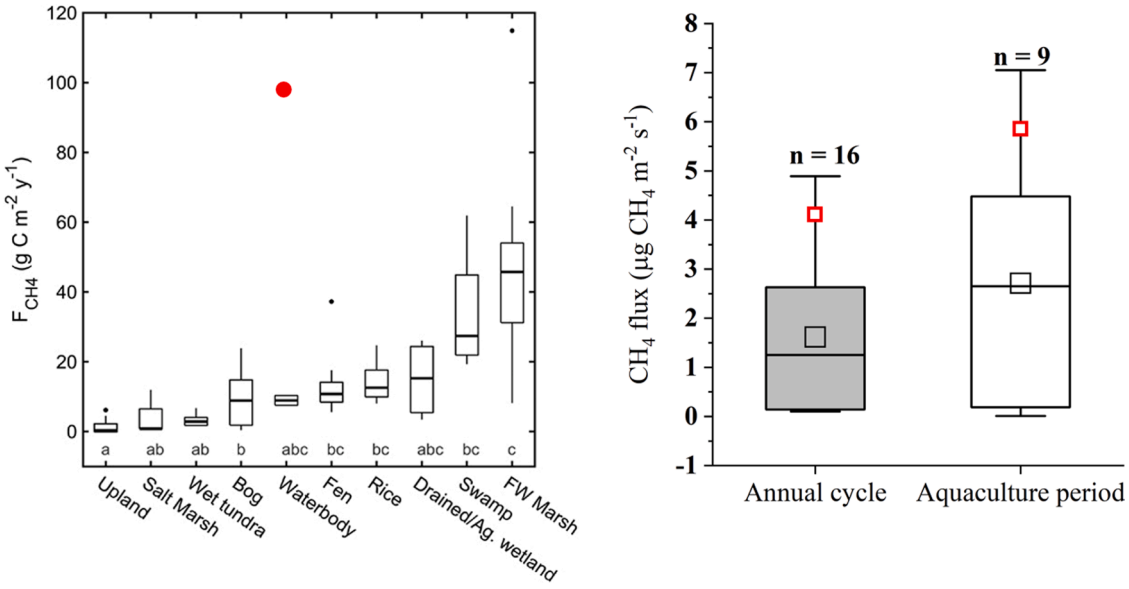


**Fig. 14.** (a) Annual $CH_4$ flux measured with the EC method reported for 10 ecosystem types according to the data provided by Knox et al. (2019). The present result is shown as the red solid circle. (b) $CH_4$ flux for freshwater aquaculture ponds based on published literature (Table S1). The top and bottom of the box indicate the 25$^{th}$ and the 75$^{th}$ quartile respectively. The line within each box and the empty square represent the median and mean, respectively. Whiskers mark the minimum and maximum values. The red square indicates the mean result from this study.

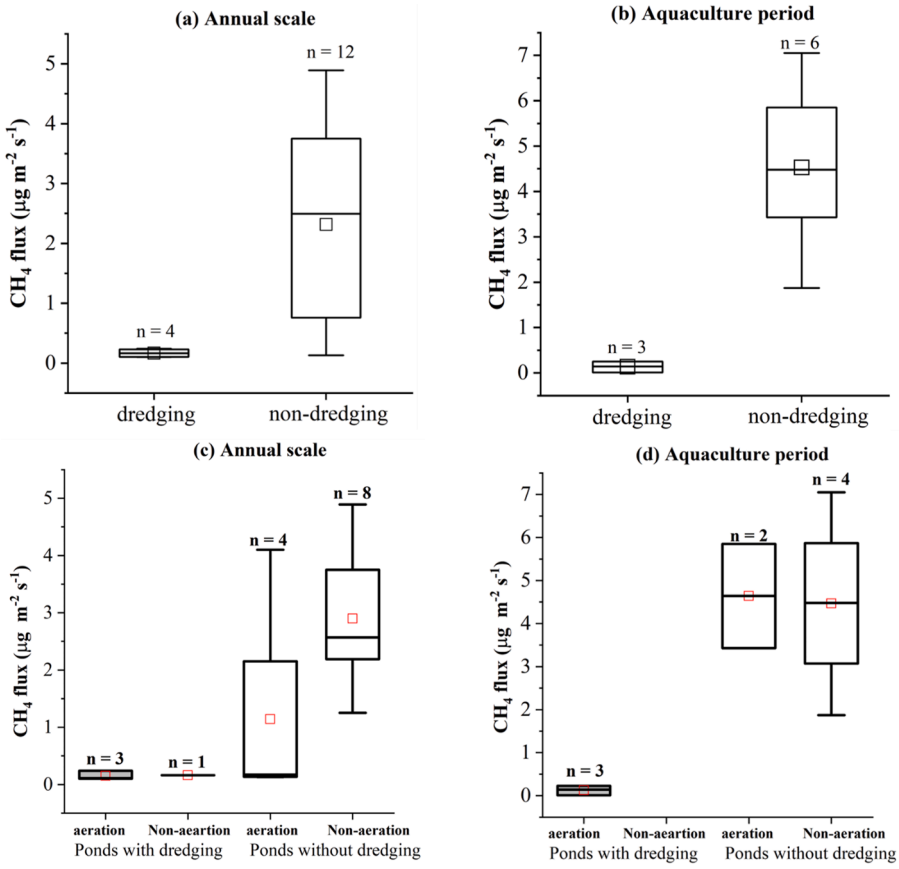


**Fig. 15.** $CH_4$ fluxes under different farming practices. The top and bottom of the box indicate the 25$^{th}$ and the 75$^{th}$ quartile, respectively. The line within each box and the empty square represents the median and mean, respectively. Whiskers mark the minimum and maximum values. Also shown is number of sites (n) in each data group.

chamber- and funnel-based studies.

## Declaration of Competing Interest

The authors declare that they have no known competing financial interests or personal relationships that could have appeared to influence the work reported in this paper.

## Acknowledgements

This research was supported by the National Natural Science Foundation of China (grant numbers 42021004, 41575147 and 41975143 to MZ and WX), the National Key R&D Program of China (grant number 2020YFA0607501 to WX and MZ, grant number 2017YFC0209700 to ZF) and open fund from the Key Laboratory of Meteorology and Ecological Environment of Hebei Province (Z201901H to WX).

## Supplementary materials

Supplementary material associated with this article can be found, in the online version, at doi:10.1016/j.agrformet.2021.108600.

## References

Adhikari, S., Lal, R., Sahu, B.C., 2012. Carbon sequestration in the bottom sediments of aquaculture ponds of Orissa, India. Ecol. Eng. 47, 198–202.
Adhikari, S., Sarkar, S., Mandal, R.N., Rathod, R., Pillai, B.R., 2020. Assessment of Green House Gases (GHGS) Emission from Some Aquaculture Ponds of Andhra Pradesh and West Bengal, India. J. Biomed. Res. Environ. Sci. 1 (6), 241–245.
Baldocchi, D.D., Hicks, B.B., Meyers, T.P., 1988. Measuring biosphere-atmosphere exchanges of biologically related gases with micrometeorological methods. Ecology 69 (5), 1331–1340.
Baldocchi, D.D., 2020. How eddy covariance flux measurements have contributed to our understanding of Global Change Biology. Global Change Biol. 26 (1), 242–260.
Bastviken, D., Cole, J., Pace, M., Tranvik, L., 2004. Methane emissions from lakes: Dependence of lake characteristics, two regional assessments, and a global estimate. Glob. Biogeochem. Cycles 18 (4). https://doi.org/10.1029/2004GB002238.
Boyd, C.E., Wood, C.W., Chaney, P.L., Queiroz, J.F., 2010. Role of aquaculture pond sediments in sequestration of annual global carbon emissions. Environ. Pollut. 158 (8), 2537–2540.
Chaichana, N., Bellingrath-Kimura, S., Komiya, S., Fujii, Y., Noborio, K., Dietrich, O., Pakoktom, T., 2018. Comparison of closed chamber and eddy covariance methods to improve the understanding of methane fluxes from rice paddy fields in japan. Atmosphere 9 (9), 356.
Chen, H., Wu, N., Yao, S., Gao, Y., Zhu, D., Wang, Y., 2009. High methane emissions from a littoral zone on the qinghai-tibetan plateau. Atmos. Environ. 43 (32), 4995–5000.
Chen, X., Wang, Y., Sun, T., Huang, Y., Chen, Y., Zhang, M., Ye, C., 2021. Effects of Sediment Dredging on Nutrient Release and Eutrophication in the Gate-Controlled Estuary of Northern Taihu Lake. J. Chem. https://doi.org/10.1155/2021/7451832.
Cole, J.J., Caraco, N.F., 1998. Atmospheric exchange of carbon dioxide in a low-wind oligotrophic lake measured by the addition of SF6. Limnol. Oceanogr. 43 (4), 647–656.
Denfeld, B.A., Lupon, A., Sponseller, R.A., Laudon, H., Karlsson, J., 2020. Heterogeneous $CO_2$ and $CH_4$ patterns across space and time in a small boreal lake. Inland Waters 10 (3), 348–359.
Erkkilä, K.M., Ojala, A., Bastviken, D., Biermann, T., Heiskanen, J.J., Lindroth, A., Peltola, O., Rantakari, M., Vesala, T., Mammarella, I., 2018. Methane and carbon dioxide fluxes over a lake: comparison between eddy covariance, floating chambers and boundary layer method. Biogeosciences 15 (2), 429–445.
Eugster, W., DelSontro, T., Sobek, S., 2011. Eddy covariance flux measurements confirm extreme $CH_4$ emissions from a Swiss hydropower reservoir and resolve their short-term variability. Biogeosciences 8 (9), 2815–2831.
FAO. 2020. The State of World Fisheries and Aquaculture 2020 – Sustainability in action. Rome. https://doi.org/10.4060/ca9229en.
Goodrich, J.P., Varner, R.K., Frolking, S., Duncan, B.N., Crill, P.M., 2011. High-frequency measurements of methane ebullition over a growing season at a temperate peatland site. Geophys. Res. Lett. 38 (7) https://doi.org/10.1029/2011GL046915.
Helbig, M., Wischnewski, K., Gosselin, G.H., Biraud, S.C., Bogoev, I., Chan, W.S., Euskirchen, E.S., Glenn, A.J., Marsh, P.M., Quinton, W.L., Sonnentag, O., 2016. Addressing a systematic bias in carbon dioxide flux measurements with the EC150 and the IRGASON open-path gas analyzers. Agric. For. Meteorol. 228, 349–359.
Hu, Z.Q., Wu, S., Ji, C., Zou, J.W., Zhou, Q.S., Liu, S.W., 2016. A comparison of methane emissions following rice paddies conversion to crab-fish farming wetlands in southeast China. Environ. Sci. Pollut. Res. 23 (2), 1505–1515.
Kamula, C.M., Macdonald, R.W., Kuzyk, Z.Z.A., 2020. Sediment and particulate organic carbon budgets of a subarctic estuarine fjard: lake melville, labrador. Mar. Geol. 424, 106154 https://doi.org/10.1016/j.margeo.2020.106154.
Kim, Y., Johnson, M.S., Knox, S.H., Black, T.A., Dalmagro, H.J., Kang, M., Kim, J., Baldocchi, D., 2020. Gap-filling approaches for eddy covariance methane fluxes: A comparison of three machine learning algorithms and a traditional method with principal component analysis. Global Change Biol. 26 (3), 1499–1518.
Kljun, N., Calanca, P., Rotach, M.W., Chmid, H.P., 2015. A simple two-dimensional parameterization for Flux Footprint Prediction (FFP). Geosci. Model Dev. 8 (11), 3695–3713.
Knox, S.H., Jackson, R.B., Poulter, B., McNicol, G., Fluet-Chouinard, E., Zhang, Z., Zona, D., et al., 2019. FLUXNET-$CH_4$ synthesis activity: Objectives, observations, and future directions. Bull. Am. Meteorol. Soc. 100 (12), 2607–2632.
Kosten, S., Berg, S.V.D., Mendonça, R., Paranaíba, J.R., Roland, F., Sobek, S., Hoek, J.V. D., Barros, N., 2018. Extreme drought boosts $CO_2$ and $CH_4$ emissions from reservoir drawdown areas. Inland Waters. https://doi.org/10.1080/20442041.2018.1483126.
Kosten, S., Almeida, R.M., Barbosa, I., Mendonça, R., Muzitano, I.S., Oliveira-Junior, E. S., Vroom, R.J., Wang, H.J., Barros, N., 2020. Better assessments of greenhouse gas emissions from global fish ponds needed to adequately evaluate aquaculture footprint. Sci. Total Environ. 748, 141247.
Lee, X.H, Massman, W., Law, B, 2004. Handbook of Micrometeorology: A Guide for Surface Flux Measurement and Analysis, Vol. 29. Springer Science & Business Media.
Liu, S.W., Hu, Z.Q., Wu, S., Li, S.Q., Li, Z.F., Zou, J.W., 2016. Methane and nitrous oxide emissions reduced following conversion of rice paddies to inland crab–fish aquaculture in Southeast China. Environ. Sci. Technol. 50 (2), 633–642.
Loken, L.C., Crawford, J.T., Schramm, P.J., Stadler, P., Desai, A.R., Stanley, E.H., 2019. Large spatial and temporal variability of carbon dioxide and methane in a eutrophic lake. J. Geophys. Res. Biogeosci. 124, 2248–2266.
Lu, Y., Gao, Y., Jia, J., Xia, S.X., Wen, X.F., Yu, X.B., Shi, K., Li, Z.X., Wang, S.Y., 2021. Revealing carbon balance characteristics in a water conveyance-type lake and differences in carbon sources through its connective hydrological channels. J. Hydrol. 592 https://doi.org/10.1016/j.jhydrol.2020.125820.
Ma, Y.C., Sun, L.Y., Liu, C.Y., Yang, X.Y., Zhou, W., Yang, B., Schwenke, G., Li Liu, D., 2018. A comparison of methane and nitrous oxide emissions from inland mixed-fish and crab aquaculture ponds. Sci. Total Environ. 637, 517–523.
Mauder, M., Foken, T., 2004. Documentation and Instruction Manual of the Eddy Covariance Software Package TK2. University of Bayreuth. Department of Micrometeorology. Arbeitsergebnisse Nr. 26, 42.
McDermitt, D., Burba, G., Xu, L., Anderson, T., Komissarov, A., Riensche, B., Schedlbauer, J., Starr, G., Zona, D., Oechel, W., Oberbauer, S., Hastings, S., 2011. A new low-power, open-path instrument for measuring methane flux by eddy covariance. Appl. Phys. B 102 (2), 391–405.
Meijide, A., Manca, G., Goded, I., Magliulo, V., Di, T.P., Seufert, G., Cescatti, A., 2011. Seasonal trends and environmental controls of methane emissions in a rice paddy field in northern Italy. Biogeosci. Discuss. 8 (12), 3809–3821.
Moncrieff, J.B., Massheder, J.M., De Bruin, H., Elbers, J., Friborg, T., Heusinkveld, B., Kabat, P., Scott, S., Søgaard, H., Verhoef, A., 1997. A system to measure surface fluxes of momentum, sensible heat, water vapour and carbon dioxide. J. Hydrol. 188, 589–611.
Morgenstern, K., Black, T.A., Humphreys, E.R., Griffis, T.J., Drewitt, G.B., Cai, T., Nesic, Z., Spittlehouse, D.L., Livingston, N.J., 2004. Sensitivity and uncertainty of the carbon balance of a Pacific Northwest Douglas-fir forest during an El Niño/La Niña cycle. Agric. For. Meteorol. 123 (3–4), 201–219.
Natchimuthu, S., Sundgren, I., Gålfalk, M., Klemedtsson, L., Crill, P., Danielsson, Å., Bastviken, D., 2015. Spatio-temporal variability of lake $CH_4$ fluxes and its influence on annual whole lake emission estimates. Limnology & Oceanography 61. https://doi.org/10.1002/lno.10222.
Papale, D., Reichstein, M., Aubinet, M., Canfora, E., Bernhofer, C., Kutsch, W., Longdoz, B., Rambal, S., Valentini, R., Vesala, T., Yakir, D., 2006. Towards a standardized processing of Net Ecosystem Exchange measured with eddy covariance technique: algorithms and uncertainty estimation. Biogeosciences 3 (4), 571–583.
Peacock, M., Audet, J., Bastviken, D., Cook, S., Evans, C.D., Grinham, A., Holgerson, M. A., Högbom, L., Pickard, A.E., Zieliński, P., Futter, M.N., 2021. Small artificial waterbodies are widespread and persistent emitters of methane and carbon dioxide. Global Change Biol. https://doi.org/10.1111/GCB.15762.
Podgrajsek, E., Sahlée, E., Rutgersson, A., 2014. Diurnal cycle of lake methane flux. J. Geophys. Res. Biogeosci. 119, 236–248.
Reba, M.L., Fong, B.N., Rijal, I., Adviento-Borbe, M.A., Chiu, Y.L., Massey, J.H., 2020. Methane flux measurements in rice by static flux chamber and eddy covariance. Agrosyst. Geosci. Environ. 3 (1), e20119.
Rey-Sanchez, A.C., Morin, T.H., Stefanik, K.C., Wrighton, K., Bohrer, G., 2018. Determining total emissions and environmental drivers of methane flux in a Lake Erie estuarine marsh. Ecol. Eng. 114, 7–15.
Rosentreter, J.A., Borges, A.V., Deemer, B.R., Holgerson, M.A., Liu, S.D., Song, C.L., Melack, J., Raymond, P.A., Duarte, C.M., Allen, G.H., Olefeldt, D., Poulter, B., Battin, T.I., Eyre, B.D., 2021. Half of global methane emissions come from highly variable aquatic ecosystem sources. Nat. Geosci. 14, 225–230.
Sass, R.L., 2003. $CH_4$ emissions from rice agriculture. Good practice guidance and uncertainty management in national greenhouse gas inventories. IPCC Rep. 399–417.
Saunois, M., Stavert, A.R., Poulter, B., Bousquet, P., Canadell, J.G., Jackson, R.B., et al., 2020. The global methane budget 2000–2017. Earth Syst. Sci. Data 12 (3), 1561–1623.
Schubert, C.J., Diem, T., Eugster, W., 2012. Methane emissions from a small wind shielded lake determined by eddy covariance, flux chambers, anchored funnels, and boundary model calculations: a comparison. Environ. Sci. Technol. 46 (8), 4515–4522.
Tanner, C.B., Thurtell, G.W., 1969. Anemoclinometer measurements of Reynolds stress and heat transport in the atmospheric surface layer. Wisconsin Univ-Madison Dept of Soil Science.

Tuovinen, J.P., Aurela, M., Hatakka, J., Räsänen, A., Virtanen, T., Mikola, J., Ivakhov, V., Kondratyev, V., Laurila, T., 2019. Interpreting eddy covariance data from heterogeneous siberian tundra: land cover-specific methane fluxes and spatial representativeness. Biogeosci. Discuss. 16, 255–274.

Urban, N.R., Auer, M.T., Green, S.A., Lu, X., Apul, D.S., Powell, K.D., Bub, L., 2005. Carbon cycling in Lake Superior. J. Geophys. Res. Oceans 110 (C6), C06S90. https://doi.org/10.1029/2003JC002230.

Wang, H., Lu, J.W., Wang, W.D., Yang, L.Y., Yin, C.Q., 2006. Methane fluxes from the littoral zone of hypereutrophic Taihu Lake, China. J. Geophys. Res. 111, D17109. https://doi.org/10.1029/2005JD006864.

Webb, E.K., Pearman, G.I., Leuning, R., 1980. Correction of flux measurements for density effects due to heat and water vapour transfer. Q. J. R. Meteorolog. Soc. 106 (447), 85–100.

Werle, P.W., 1999. Eddy correlation measurements of methane fluxes from Italian rice-paddy fields. In: Application of Tunable Diode and Other Infrared Sources for Atmospheric Studies and Industrial Processing Monitoring II, 3758, pp. 41–52.

Werle, P., Kormann, R., 2001. Fast chemical sensor for eddy-correlation measurements of methane emissions from rice paddy fields. Appl. Opt. 40 (6), 846.

Wik, M., Crill, P.M., Varner, R.K., Bastviken, D., 2013. Multiyear measurements of ebullitive methane flux from three subarctic lakes. J. Geophys. Res. Biogeosci. 118 (3), 1307–1321.

Wik, M., Varner, R.K., Anthony, K.W., Macintyre, S., Bastviken, D., 2016. Climate-sensitive northern lakes and ponds are critical components of methane release. Nat. Geosci. https://doi.org/10.1038/NGEO2578.

Wu, S., Hu, Z.Q., Hu, T., Chen, J., Yu, K., Zou, J.W., Liu, S.W., 2018. Annual methane and nitrous oxide emissions from rice paddies and inland fish aquaculture wetlands in southeast China. Atmos. Environ. 175, 135–144.

Xiao, S.B., Yang, H., Liu, D.F., Zhang, C., Lei, D., Wang, Y.C., Peng, F., Li, Y.C., Wang, C. H., Li, X.L., Wu, G.C., Liu, L., 2014. Gas transfer velocities of methane and carbon dioxide in a subtropical shallow pond. Tellus B Chem. Phys. Meteorol. 66 (1), 23795.

Xiao, Q.T., Zhang, M., Hu, Z.H., Gao, Y.Q., Hu, C., Liu, C., Liu, S.D., Zhang, Z., Zhao, J.Y., Xiao, W., Lee, X.H., 2017. Spatial variations of methane emission in a large shallow eutrophic lake in subtropical climate. J. Geophys. Res. Biogeosci. 122 (7), 1597–1614.

Yang, P., Lai, D.Y., Huang, J.F., Tong, C., 2017. Effect of drainage on $CO_2$, $CH_4$, and $N_2O$ fluxes from aquaculture ponds during winter in a subtropical estuary of China. J. Environ. Sci. 65, 72–82.

Yang, P., Zhang, Y.F., Lai, D.Y., Tan, L.S., Jin, B.S., Tong, C., 2018. Fluxes of carbon dioxide and methane across the water–atmosphere interface of aquaculture shrimp ponds in two subtropical estuaries: The effect of temperature, substrate, salinity and nitrate. Sci. Total Environ. 635, 1025–1035.

Yang, P., Zhang, Y., Yang, H., Zhang, Y.F., Xu, J., Tan, L.S., Tong, C., Lai, D.Y., 2019. Large fine-scale spatiotemporal variations of $CH_4$ diffusive fluxes from shrimp aquaculture ponds affected by organic matter supply and aeration in Southeast China. J. Geophys. Res. Biogeosci. 124 (5), 1290–1307.

Yang, P., Zhang, Y.F., Yang, H., Guo, Q.Q., Lai, D.Y., Zhao, G.H., Li, L., Tong, C., 2020. Ebullition was a major pathway of methane emissions from the aquaculture ponds in southeast China. Water Res. 184 https://doi.org/10.1016/j.watres.2020.116176.

Yuan, J.J., Xiang, J., Liu, D.Y., Kang, H., He, T.H., Kim, S., Lin, Y.X., Freeman, C., Ding, W.X., 2019. Rapid growth in greenhouse gas emissions from the adoption of industrial-scale aquaculture. Nature Climate Change 9 (4), 18–322.

Yuan, J.J., Liu, D.Y., Xiang, J., He, T.H., Kang, H.J., Ding, W.X., 2021. Methane and nitrous oxide have separated production zones and distinct emission pathways in freshwater aquaculture ponds. Water Res. 190. https://doi.org/10.1016/j.watres.2020.116739.

Zhang, M., Xiao, Q.T., Zhang, Z., Gao, Y.Q., Zhao, J.Y., Pu, Y.N., Wang, W., Xiao, W., Liu, S.D., Lee, X.H., 2019. Methane flux dynamics in a submerged aquatic vegetation zone in a subtropical lake. Sci. Total Environ. 672, 400–409.

Zhao, H.C., Jia, G., Wang, H., Zhang, A., Xu, X., 2019a. Seasonal and interannual variations in carbon fluxes in East Asia semi-arid grasslands. Sci. Total Environ. 668, 1128–1138.

Zhao, J.Y., Zhang, M., Xiao, W., Wang, W., Zhang, Z., Yu, Z., Xiao, Q.T., Cao, Z.D., Xu, J. Z., Zhang, X.F., Liu, S.D., Lee, X.H., 2019b. An evaluation of the flux-gradient and the eddy covariance method to measure $CH_4$, $CO_2$, and $H_2O$ fluxes from small ponds. Agric. For. Meteorol. 275, 255–264.